



## Transformation of seismic velocity data to extract porosity and saturation values for rocks

James G. Berryman,<sup>1</sup> Patricia A. Berge,<sup>2</sup> and Brian P. Bonner<sup>3</sup>

### ABSTRACT

For wave propagation at low frequencies in a porous medium, the Gassmann-Domenico relations are well-established for homogeneous partial saturation by a liquid. They provide the correct relations for seismic velocities in terms of constituent bulk and shear moduli, solid and fluid densities, porosity and saturation. It has not been possible, however, to invert these relations easily to determine porosity and saturation when the seismic velocities are known. Also, the state (or distribution) of saturation, *i.e.*, whether or not liquid and gas are homogeneously mixed in the pore space, is another important variable for reservoir evaluation. A reliable ability to determine the state of saturation from velocity data continues to be problematic. We show how transforming compressional and shear wave velocity data to the  $(\rho/\lambda, \mu/\lambda)$ -plane (where  $\lambda$  and  $\mu$  are the Lamé parameters and  $\rho$  is the total density) results in a set of quasi-orthogonal coordinates for porosity and liquid saturation that greatly aids in the interpretation of seismic data for the physical parameters of most interest. A second transformation of the same data then permits isolation of the liquid saturation value, and also provides some direct information about the state of saturation. By thus replotting the data in the  $(\lambda/\mu, \rho/\mu)$ -plane, inferences can be made concerning the degree of patchy (inhomogeneous) versus homogeneous saturation that is present in the region of the medium sampled by the data. Our examples include igneous and sedimentary rocks, as well as man-made porous materials. These results have potential applications in various areas of interest, including petroleum exploration and reservoir characterization, geothermal resource evaluation, environmental restoration monitoring, and geotechnical site characterization.

### INTRODUCTION

In a variety of applied problems, it is important to determine the state of saturation of a porous medium from acoustic or seismic measurements. In the oil and gas industry, it is common to use amplitude-versus-offset (AVO) processing of seismic reflection data to reach conclusions about the presence of gas, oil, and their relative abundances on the opposite sides of a

<sup>1</sup>**email:** berryman@sep.stanford.edu

<sup>2</sup>Lawrence Livermore National Lab, P. O. Box 808, L-201, Livermore, CA 94550  
**email:** berge1@llnl.gov

<sup>3</sup>Lawrence Livermore National Lab, P. O. Box 808, L-201, Livermore, CA 94550  
**email:** bonner1@llnl.gov

reflecting interface underground [*e.g.*, Castagna and Backus (1993)]. For environmental applications, we can expect to be working in the near surface where sensor geometries other than surface reflection surveys become practical. For example, when boreholes are present, it is possible to do crosswell seismic tomography, or borehole sonic logging to determine velocities [*e.g.*, Harris *et al.* (1995)]. For AVO processing the data obtained are the seismic impedances  $\rho v_p$  and  $\rho v_s$  (where  $\rho$  is the density, and  $v_p, v_s$  are the seismic compressional and shear wave velocities, respectively), which arise naturally in reflectance measurements. (In this paper, we will use the term “velocities” to refer to measured velocities at seismic, sonic, or ultrasonic frequencies, unless otherwise specified.) However, for crosswell applications, we are more likely to have simply velocity data, *i.e.*,  $v_p$  and  $v_s$  themselves without density information. For well-logging applications, separate measurements of the velocities as well as density are possible. Although a great deal of effort has been expended on AVO analysis, relatively little has been done to invert the simple velocity data for porosity and saturation. It is our purpose to present one method that shows promise for using velocity data to obtain porosity and saturation estimates. The key physical idea used here is the fact that the Lamé parameter  $\lambda$  and the density  $\rho$  are the two parameters containing information about saturation, while both of these together with shear modulus  $\mu$  contain information about porosity ( $\lambda$  and  $\mu$  are defined in the next section). These facts are well-known from earlier work of Gassmann (1951), Domenico (1974), and many others. (It is well-established that even though the Gassmann-Domenico relations are derived for the static case, they have been found to describe behavior measured in the field at sonic and seismic frequencies, and, in some cases, even in laboratory ultrasonic experiments.) The same facts are used explicitly in AVO analysis (Castagna and Backus, 1993; Ostrander, 1984; Castagna *et al.*, 1985; Foster *et al.*, 1997), but in ways that are significantly different from those to be described here. A major point of departure is that the present work allows direct information to be obtained about, not only the level of the saturation, but also concerning the state of saturation, *i.e.*, whether the liquid and gas present are mixed homogeneously, or are instead physically separated and therefore in a state of patchy saturation (Berryman *et al.*, 1988; Endres and Knight, 1989; Knight and Nolen-Hoeksema, 1990; Mavko and Nolen-Hoeksema, 1994; Dvorkin and Nur, 1998; Cadoret *et al.*, 1998). Another advantage is that this method uses velocity rather than amplitude information, and therefore may have less uncertainty and may also require less data processing for some types of field experiments.

One of the main points of the analysis to be presented is the purposeful avoidance of the well-known complications that arise at high frequencies, due in large part to velocity dispersion and attenuation (Biot, 1956a,b; Biot, 1962; O’Connell and Budiansky, 1977; Mavko and Nur, 1978; Berryman, 1981; McCann and McCann, 1985; Johnson *et al.*, 1987; Norris, 1993; Best and McCann, 1995). Our point of view is that seismic data (as well as most sonic, and some ultrasonic data) do not suffer from contamination by the frequency-dependent effects to the same degree typically seen for high frequency laboratory measurements. By restricting our range of frequencies to those most useful in the field, we anticipate a significant simplification of the analysis and therefore an improvement in our ability to provide both simple and robust interpretations of field data. In the Discussion section, we also provide a means of identifying data in need of correction for dispersion effects.

We introduce the basic physical ideas in the next section. Then we present two new meth-

ods of displaying the velocity data. One method is used to sort data points into sets that have similar physical attributes, such as porosity. Then, the second method is used to identify both the level of saturation and the type of saturation, whether homogeneous, patchy, or a combination of the two. We show a subset of the large set of data we have examined that confirms these conclusions empirically. We then provide some discussion of the results and what we foresee as possible future applications of the ideas. Finally, we summarize the accomplishments of the paper in the concluding section.

## ELASTIC AND POROELASTIC WAVE PROPAGATION

For isotropic elastic materials there are two bulk elastic wave speeds (Aki and Richards, 1980), compressional  $v_p = \sqrt{(\lambda + 2\mu)/\rho}$  and shear  $v_s = \sqrt{\mu/\rho}$ . Here  $\rho$  is the overall density, and the Lamé parameters  $\lambda$  and  $\mu$  are the constants that appear in Hooke's law relating stress to strain in an isotropic material. The constant  $\mu$  gives the dependence of shear stress on shear strain in the same direction. The constant  $\lambda$  gives the dependence of compressional or tensional stress on extensional or dilatational strains in orthogonal directions. For a porous system with porosity  $\phi$  (void volume fraction) in the range  $0 < \phi < 1$ , the overall density of the rock or sediment is just the volume weighted density given by

$$\rho = (1 - \phi)\rho_s + \phi[S\rho_l + (1 - S)\rho_g], \quad (1)$$

where  $\rho_s$ ,  $\rho_l$ ,  $\rho_g$  are the densities of the constituent solid, liquid and gas, respectively.  $S$  is the liquid saturation, *i.e.*, the fraction of liquid-filled void space in the range  $0 \leq S \leq 1$  [see Domenico (1974)]. When liquid and gas are distributed uniformly in all pores and cracks, Gassmann's equations say that, for quasistatic isotropic elasticity and low frequency wave propagation, the shear modulus  $\mu$  will be mechanically independent of the properties of any fluids present in the pores, while the overall bulk modulus  $K$  ( $\equiv \lambda + \frac{2}{3}\mu$ ) of the rock or sediment including the fluid depends in a known way on porosity and elastic properties of the fluid and dry rock or sediment (Gassmann, 1951; Berryman, 1999). Thus, in the Gassmann model, the Lamé parameter  $\lambda$  is elastically *dependent* on fluid properties, while  $\mu$  is not. The density  $\rho$  also depends on saturation, as shown in equation (1). At low liquid saturations, the bulk modulus of the fluid mixture is dominated by the gas, and therefore the effect of the liquid on  $\lambda$  is negligible until the porous medium approaches full saturation. This means that both velocities  $v_p$  and  $v_s$  will decrease with increasing fluid saturation (Domenico, 1974) due to the "density effect," wherein the only quantity changing is the density, which increases in the denominators of both  $v_p^2$  and  $v_s^2$ . As the medium approaches full saturation, the shear velocity continues its downward trend, while the compressional velocity suddenly (over a very narrow range of saturation values) shoots up to its full saturation value. A well-known example of this behavior was provided by Murphy (1984). Figure 1 shows how plots of these data for sandstones will appear in several choices of display, with Figure 1(a) being one of the more common choices. This is the expected (ideal Gassmann-Domenico) behavior of partially saturated porous media. The Gassmann-Domenico relations hold for frequencies low enough (sonic and below) that the solid frame and fluid will move in phase, in response to applied stress or displacement. The fluid pressure must be (at least approximately) uniform

throughout the porous medium, from which assumption follows the homogeneous saturation requirement.

## PREDICTIONS OF THE THEORY AND EXAMPLES

### Gassmann-Domenico relations

Gassmann's equations (Gassmann, 1951) for fluid substitution state that

$$K = K_{dr} + \frac{\alpha^2}{(\alpha - \phi)/K_m + \phi/K_f} \quad \text{and} \quad \mu = \mu_{dr}, \quad (2)$$

where  $K_m$  is the bulk modulus of the single solid mineral,  $K_{dr}$  and  $\mu_{dr}$  are the bulk and shear moduli of the drained porous frame. The special combination of moduli defined by  $\alpha = 1 - K_{dr}/K_m$  is the Biot-Willis parameter (Biot and Willis, 1957). The porosity is  $\phi$ , while  $K$  and  $\mu$  are the effective bulk and shear moduli of the undrained porous medium that is saturated with a fluid mixture having bulk modulus  $K_f$ . For partial saturation conditions with homogeneous mixing of liquid and gas, so that all pores contain the same relative proportions of liquid and gas, Domenico (1974) among others shows that

$$1/K_f = S/K_l + (1 - S)/K_g. \quad (3)$$

The saturation level of liquid is  $S$  lying in the range  $0 \leq S \leq 1$ . The bulk moduli are:  $K_l$  for the liquid, and  $K_g$  for the gas. When  $S$  is small, (3) shows that  $K_f \simeq K_g$ , since  $K_g \ll K_l$ . As  $S \rightarrow 1$ ,  $K_f$  remains close to  $K_g$  until  $S$  closely approaches unity. Then,  $K_f$  changes rapidly (over a small range of saturations) from  $K_g$  to  $K_l$ . (Note that the value of  $K_l$  may be several orders of magnitude larger than  $K_g$ , as in the case of water and air — 2.25 GPa and  $1.45 \times 10^{-4}$  GPa, respectively.)

Since  $\mu$  has no mechanical dependence on the fluid saturation, it is clear that all the fluid dependence of  $K = \lambda + \frac{2}{3}\mu$  in (2) resides within the Lamé parameter  $\lambda$ . Other recent work (Berryman *et al.*, 1999) on layered elastic media indicates that  $\lambda$  should be considered as an important independent variable for analysis of wave velocities and Gassmann's results provide some confirmation of this deduction (and furthermore provided a great deal of the motivation for the present line of research). The parameters  $K (= \lambda + \frac{2}{3}\mu)$  and  $K_{dr} (= \lambda_{dr} + \frac{2}{3}\mu_{dr})$  can be replaced in (2) by  $\lambda$  and  $\lambda_{dr}$  without changing the validity of the equation. Thus, like  $K$ , for increasing saturation values,  $\lambda$  will be almost constant until the porous medium closely approaches full saturation.

Now, the first problem that arises with field data is that we usually do not know the reason why data collected at two different locations in the earth differ. It could be that the differences are all due to the saturation differences we are concentrating on in this paper. Or it could be that they are due entirely or only partly to differences in the porous solids that contain the fluids. In fact, solid differences easily can mask any fluid differences because the range of detectable solid mechanical behavior is so much greater than that of the fluids (especially when fractures are present).

It is essential to remove such differences due to solid heterogeneity. A related issue concerns differences arising due to porosity changes throughout a system of otherwise homogeneous solids. One way of doing this would be to sort our data into sets having similar porous solid matrix. For simplicity and because of the types of laboratory data sets available, we will use porosity here as our material discriminant.

TABLE 1. Monotonicity properties of the Lamé parameters  $\lambda$  and  $\mu$  and the density  $\rho$  as the porosity  $\phi$  and liquid saturation  $S$  vary.

	Lamé $\lambda$	Lamé $\mu$	Density $\rho$
$\Delta\phi$	$\frac{\partial\lambda}{\partial\phi} _S = ?$	$\frac{\partial\mu}{\partial\phi} _S < 0$	$\frac{\partial\rho}{\partial\phi} _S < 0$
$\Delta S$	$\frac{\partial\lambda}{\partial S} _\phi > 0$ (or $\simeq 0$ )	$\frac{\partial\mu}{\partial S} _\phi = 0$	$\frac{\partial\rho}{\partial S} _\phi > 0$

Considering our three main parameters,  $\lambda$ ,  $\mu$ , and  $\rho$ , we see that all three depend on porosity, but only  $\lambda$  and  $\rho$  depend on saturation. Using formulas (1)-(3), we can take partial derivatives of each of these expressions first with respect to  $\phi$  while holding  $S$  constant, and then with respect to  $S$  while holding  $\phi$  constant. For now, we are only interested in trends rather than the exact values, and these are displayed in Table 1. The trend for  $\partial\lambda/\partial S|_\phi > 0$  requires the additional reminder that, although this term is always positive, its value is often so small that it may be treated as zero except in the small range of values close to  $S = 1$ . Also, using Hashin-Shtrikman bounds (Hashin and Shtrikman, 1962) as a guide, it turns out that it is not possible to make a general statement about the sign of  $\partial\lambda/\partial\phi|_S$ , since the result depends on the particular material constants. (Related differences of sign are also observed in the data we show later in this paper; thus, this ambiguity is definitely real and observable.)

Assuming that the primary variables are  $\lambda$ ,  $\mu$ , and  $\rho$  (further justification of this choice of primary variables is provided later in the paper), then the two pieces of velocity data we have can be used to construct the following three ratios:

$$\frac{\mu}{\lambda} = \frac{v_s^2}{v_p^2 - 2v_s^2}, \quad (4)$$

$$\frac{\rho}{\lambda} = \frac{1}{v_p^2 - 2v_s^2}, \quad (5)$$

and

$$\frac{\rho}{\mu} = \frac{1}{v_s^2}. \quad (6)$$

We will consider first of all what happens to these ratios for homogeneous mixing of fluids, and then consider the simpler case of ideal patchy saturation, where some pores in the partially saturated medium are completely filled with liquid and others are completely dry (or filled with gas).

### Homogeneous saturation

For homogeneous saturation, as  $S$  varies while porosity remains fixed, the ratio  $\mu/\lambda$  does not change significantly until  $S \rightarrow 1$ . At that point,  $\lambda$  increases dramatically and  $\mu/\lambda$  therefore decreases dramatically. Similarly, as  $S \rightarrow 1$ , the only changes in  $\rho/\lambda$  over most of the dynamic range of  $S$  are in  $\rho$ , which increases linearly with  $S$ . Then, when  $\rho$  is almost at its maximum value,  $\lambda$  increases dramatically, causing the  $\rho/\lambda$  ratio to decrease dramatically. Thus,  $\rho/\lambda$  does not change monotonically with  $S$ , but first increases a little and then decreases a lot. These two ratios may be conveniently compared by plotting data from various rocks and man-made porous media examples in the  $(\rho/\lambda, \mu/\lambda)$ -plane [see Figure 1(b) and Figure 2]. We see that, when data are collected at approximately equal intervals in  $S$ , the low saturation points will all cluster together with nearly constant  $\mu/\lambda$  and small increases in  $\rho/\lambda$ , but the final steps as  $S \rightarrow 1$  lead to major decreases in both ratios. The resulting plots appear as nearly straight lines in this plane, with drained samples plotting to the upper right and fully saturated samples plotting to the lower left in each of the examples shown in Figure 2. The remaining ratio  $\rho/\mu$  has the simplest behavior, since  $\rho$  increases monotonically in  $S$ , and  $\mu$  does not change. So  $\rho/\mu$  is a monotonically increasing function of  $S$ , and therefore can be considered a useful proxy of the saturation variable  $S$ . [Compare Figures 1(c) and 1(d), and see Figure 3.]

Figure 2(a) includes the same sandstone data from Figure 1, along with other sandstone data. Similar data for five limestone samples (Cadoret *et al.*, 1998) are plotted in Figure 2(b). The straight line correlation of the data in the sandstone display is clearly reconfirmed by the limestone data. Numerous other examples of the correlation have been observed. [Fully dry and fully saturated examples are shown here for some of these examples in Figures 2(c) and 2(d), for which partial saturation data were unavailable.] No examples of appropriate data for partially saturated samples have exhibited major deviations from this behavior, although an extensive survey of available data sets has been performed for materials including limestones (Cadoret *et al.*, 1998), sandstones (Murphy, 1984; Knight and Nolen-Hoeksema, 1990), granites (Nur and Simmons, 1969), unconsolidated sands, and some artificial materials such as ceramics and glass beads (Berge *et al.*, 1995). This straight line correlation is a very robust feature of partial saturation data. The mathematical trick that brings about this behavior will now be explained.

Consider the behavior as  $\phi$  increases for fixed  $S$ . Two of the parameters ( $\mu$  and  $\rho$ ) decrease as  $\phi$  increases, but at different rates, while the third ( $\lambda$ ) can have arbitrary variation. [Recall (Bourbié *et al.*, 1987) that rigorous bounds on the parameters are:  $0 \leq K < \infty$ ,  $0 \leq \mu < \infty$ ,  $0 < \rho < \infty$ , and  $-\frac{2}{3}\mu \leq \lambda \leq \infty$ .] To understand the behavior on these plots in Figure 1 as  $\phi$  changes, it will prove convenient to consider polar coordinates  $(r, \theta)$ , defined by

$$r^2 = w^4 \left( \frac{\rho}{\lambda} \right)^2 + \left( \frac{\mu}{\lambda} \right)^2, \quad (7)$$

and

$$\tan\theta = \frac{\mu}{\rho w^2}, \quad (8)$$

where  $w$  is an arbitrary scale factor with dimensions of velocity (chosen so that  $r$  is a dimensionless radial coordinate for plots like those in Figure 1). Now, if in addition we choose  $w$  to be sufficiently large so that  $v_s/w \ll 1$  for typical values of  $v_s$  in our data sets, then, using standard perturbation expansions, we have

$$r = \frac{\rho}{\lambda} w^2 \left(1 + \frac{v_s^4}{w^4}\right)^{\frac{1}{2}} \simeq \frac{\rho}{\lambda} w^2 \left(1 + \frac{v_s^4}{2w^4}\right) \quad (9)$$

and

$$\theta = \tan^{-1} \left( \frac{v_s^2}{w^2} \right) \simeq \frac{v_s^2}{w^2}. \quad (10)$$

Thus, the angle  $\theta$  is well approximated by the ratio in (10), which depends only on the shear velocity  $v_s$ . We know the shear velocity is a rather weak function of saturation [*e.g.*, Figure 1(a)], but a much stronger function of porosity [see, for example, Berge *et al.* (1995)]. So we see that the angle in these plots is most strongly correlated with changes in the porosity. In contrast, the radial position  $r$  is principally dependent on the ratio  $\rho/\lambda$ , which we have already shown to be a strong function of the saturation  $S$ , especially in the region close to full liquid saturation. This analysis shows why the plots in Figures 1(b) and 2 look the way they do and also why we might be inclined to call these quasi-orthogonal (polar) plots of saturation and porosity. Because of the function these plots play in our analysis, we will call them the “data-sorting” plots.

In contrast, the plots in Figure 3 contain information about fluid spatial distribution, as will be discussed at greater length later in this paper. The bulk modulus  $K_f$  contains the only  $S$  dependence in (2). Thus, for porous materials satisfying Gassmann’s homogeneous fluid conditions and for low enough frequencies, the theory predicts that, if we use velocity data in a two-dimensional plot with one axis being the saturation  $S$  and the other being the ratio  $\lambda/\mu = (v_p/v_s)^2 - 2$ , then the results will lie along an essentially straight (horizontal) line until the saturation reaches  $S \simeq 1$  (around 95% or higher), where the curve formed by the data will quickly rise to the value determined by the velocities at full liquid saturation. On such a plot, the drained data appear in the lower left while the fully saturated data appear in the upper right. This behavior is illustrated in Figure 3(a) for Espeil limestone. The behavior of the other plots in Figure 3 will be described below.

Before leaving this discussion of homogeneous saturation, we should note that there is one laboratory saturation technique for which it is known — from direct observations (Cadoret *et al.*, 1998) using x-ray imaging — that very homogeneous liquid-gas mixtures will generally be produced. This method is called “depressurization.” When such data are available (see Figure 3), we expect they will always behave according to the Gassmann-Domenico predictions. In contrast, the more common approach which produces drainage data is less predictable, since the manner and rate of drainage depend strongly on details of particular samples — especially



on surface energies that control capillarity and on permeability magnitude and distribution. Thus, the drainage technique can produce homogeneous saturation, or patchy saturation, or anything in between.

### Patchy saturation

The preceding analysis centered on homogeneous saturation of porous media. On the other hand, consider a porous medium containing gas and liquid mixed in a heterogeneous manner, so that patches of the medium hold only gas while other patches hold only liquid in the pores. Then, the theory predicts that, depending to some extent on the spatial distribution of the patches, the results will deviate overall from Gassmann's results (although Gassmann's results will hold locally in each individual patch). If we consider the most extreme cases of spatial distribution possible, which are laminated regions of alternating liquid saturation and gas saturation, then the effective bulk modulus will be determined by an average of the two extreme values of (2):  $K|_{S=0} = K_{dr}$  and  $K|_{S=1}$ . Using saturation as the weighting factor, the harmonic mean and the mean are the two well-known extremes of behavior (Hill, 1952). Of these two, the one that differs most from (2) for  $0 < S < 1$  is the mean. And, because of  $K$ 's linear dependence on both  $\lambda$  and  $\mu$ , and  $\mu$ 's independence of  $S$ , we therefore have

$$\lambda_{patchy}(S) = (1 - S)\lambda_{dr} + S\lambda|_{S=1}. \quad (11)$$

So, on our plot in the  $(\lambda/\mu, \rho/\mu)$ -plane, the results for the mean will again lie along a straight line, but now the line goes directly from the unsaturated value ( $S = 0$ ) to the fully saturated value ( $S = 1$ ) [*e.g.*, Figure 3(e)]. The two straight lines described [the one given by (11) and the horizontal one discussed in the preceding paragraph for saturations up to about 95%] are rigorous results of the theory, and form two sides of a triangle that will contain all data for partially saturated systems, regardless of the type of saturation present. The third side of this triangle provides a rigorous bound on the behavior as full saturation is approached (it just corresponds to the physical requirement that  $S \leq 1$ , so values with  $S > 1$  have no physical significance). In general, heterogeneous fluid distribution can produce points anywhere within the resulting triangle, but not outside the triangle (within normal experimental error).

A brief presentation of some examples (Figure 3) will now follow a reminder of an important and well-known caveat.

### Caveats for chemical effects

Some deviations from these conclusions can be expected at the lowest saturations. Chemical effects, which have not been accounted for in the mechanical analysis, can and often do lead to the situation that dry and drained (nearly dry or room dry) samples have somewhat different properties (Bonner *et al.*, 1997). These differences are larger than can be explained by mechanical analyses alone. [For example, see Figures 3(a) and 3(b). Take special note of the three lowest saturation values in these Figures.] We discuss this point at greater length in the Discussion section.

### Some illustrative examples

Figure 3 shows three examples of the results obtained with plots in the  $(S, \lambda/\mu)$ -plane and in the  $(\rho/\mu, \lambda/\mu)$ -plane (using  $\rho/\mu$  as a proxy for  $S$ ) for two limestones and one andesite from laboratory data of Cadoret (1993) and Cadoret *et al.* (1995; 1998). In Figure 3, the true saturation data are used in the Figures on the left and the proxy for saturation ( $\rho/\mu$ ) is used on the right. We therefore call the right hand diagrams “saturation-proxy” plots. Using the interpretations arising for our analysis of Gassmann-Domenico partial-saturation theory, we see that Figures 3(a) and (b) indicate homogeneous mixing of liquid and gas, while Figures 3(e) and (f) indicate extremely patchy mixing, and Figures 3(c) and (d) show an intermediate state of mixing for the drainage data, but more homogeneous mixing (as expected) for the depressurization data. The Espeil limestone was observed to be the most dispersive of all those rocks considered in the data sets of Cadoret (1993) and Carodet *et al.* (1995; 1998). So this case is a very stringent test of the method. In fact, if we were to plot the corresponding data for Espeil limestone at 500 kHz, we would not find such simple and easily interpreted behavior on these plots. Our explanation for this difference between the 500 kHz and 1 kHz results for Espeil limestone is that the dispersion introduces effects not accounted for by the simple Gassmann-Domenico theory, and that there is then no reason to think that our method should work for such high frequencies as 500 kHz. We have found other examples where it does work for frequencies higher than one might expect the method to be valid. The point is that, if we restrict the range of frequencies considered to 1 kHz or less, the method appears to work quite well on most (and perhaps all) samples. [But, at higher frequencies, the solid and fluid can move out of phase and other relations developed by Biot (1956a,b; 1962) and others (O’Connell and Budiansky, 1977; Mavko and Nur, 1978; Berryman, 1981; McCann and McCann, 1985; Johnson *et al.*, 1987; Norris, 1993; Best and McCann, 1995) apply.]

## DISCUSSION

### Rocks containing more than one mineral

The analysis presented here has been limited for simplicity to the case of single mineral porous rocks. In fact the main parts of the analysis do not change in any significant way if the rock has multiple constituents. The well-known result of Brown and Korrington (1975) states that

$$K = K_{dr} + \frac{\alpha^2}{\alpha/K_s - \phi/K_\phi + \phi/K_f} \quad \text{and} \quad \mu = \mu_{dr}, \quad (12)$$

where  $K_s$  is theunjacketed bulk modulus of the composite solid frame,  $K_\phi$  is theunjacketed pore modulus of the composite solid frame,  $\alpha = 1 - K_{dr}/K_s$  is the appropriate Biot-Willis (1957) parameter for this situation. The remaining parameters have the same significance as in (2). The functional dependence of  $K_{sat}$  on the saturation  $S$  is clearly the same in both formulas. If we were trying to infer properties of the solid from these formulas, then of course (12) would be more difficult to interpret. But for our present purposes, we are only trying to infer porosity, saturation values, and saturation state. For these physical parameters, the analysis goes through without change.

### On uniqueness of $\lambda$ -diagrams

Since the possible linear combinations of the elastic bulk and shear moduli ( $K$  and  $\mu$ ) are infinite, it is natural to ask why (or if) the choice  $\lambda = K - \frac{2}{3}\mu$  is special? Is there perhaps some other combination of these constants that works as well or even better than the choice made here? There are some rather esoteric reasons based on recent work (Berryman *et al.*, 1999) in the analysis of layered anisotropic elastic media that lead us to believe that the choice  $\lambda$  is indeed special, but we will not try to describe these reasons here. Instead we will point out some general features of the two types of plots that make it clear that this choice is generally good, even though others might be equally good or even better in special circumstances. First, in the diagram using the  $(\rho/\mu, \lambda/\mu)$ -plane, it is easy to see that *any* plot of data using linear combinations of the form  $(\rho/\mu, (\lambda + c\mu)/\mu)$ , where  $c$  is any real constant, will have precisely the same information and the display will be identical except for a translation of the values along the ordinate by the constant value  $c$ . Thus, for example taking  $c = \frac{2}{3}$ , plots of  $(\rho/\mu, K/\mu)$  will have exactly the same interpretational value as those presented here. But, if we now reconsider the data-sorting plot (*e.g.*, Figure 2) for each of these choices, we need to analyze plots of the form  $(\rho/(\lambda + c\mu), \mu/(\lambda + c\mu))$ . Is there an optimum choice of the parameter  $c$  that makes the plots as straight as possible whenever the only variable is the fluid saturation? It is not hard to see that the class of best choices always lies in the middle of the range of values of  $\lambda/\mu$  taken by the data. So setting  $-c = \frac{1}{2}(\min(\lambda/\mu) + \max(\lambda/\mu))$  will always guarantee that there are very large positive and negative values of  $\mu/(\lambda + c\mu)$ , and therefore that these data fall reliably (if somewhat approximately) along a straight line. But the minimum value of  $\lambda/\mu$  has an absolute minimum of  $-\frac{2}{3}$ , based on the physical requirement of positivity of  $K$ . So  $c < \frac{2}{3}$  is a physical requirement, and since  $\max \lambda/\mu \simeq +\frac{2}{3}$  is a fairly typical value for porous rocks, it is expected that an optimum value of  $c \leq 0$  will generally be obtained using this criterion. Thus, plots based on bulk modulus  $K$  instead of  $\lambda$  will not be as effective in producing the quasi-orthogonality of porosity and saturation that we have obtained in the data-sorting style of plotting. We conclude that the choice  $\lambda$  is not unique (some other choices might be as good for special data sets), but it is nevertheless an especially simple choice and is also expected to be quite good for most real data.

### Transforming straight lines to straight lines

One important feature concerning connections between the points in the two planes  $(\rho/\lambda, \mu/\lambda)$  and  $(\rho/\mu, \lambda/\mu)$  is the fact that (with only a few exceptions that will be noted) straight lines in one plane transform into straight lines in the other. For example, points satisfying

$$\frac{\lambda}{\mu} = A + B \frac{\rho}{\mu} \quad (13)$$

in the  $(\rho/\mu, \lambda/\mu)$ -plane (where  $A$  and  $B$  are constant intercept and slope, respectively), then satisfy

$$\frac{\mu}{\lambda} = A^{-1} - A^{-1} B \frac{\rho}{\lambda} \quad (14)$$

in the  $(\rho/\lambda, \mu/\lambda)$ -plane. So long as  $A \neq 0$  in (13), the straight line in (13) transforms into the straight line in (14). This observation is very important because the straight line in (11) corresponds to a straight line in the saturation-proxy plot in the  $(\rho/\mu, \lambda/\mu)$ -plane. But this line transforms into a straight line in data-sorting plot in the  $(\rho/\lambda, \mu/\lambda)$ -plane. In fact the apparent straight line along which the data align themselves in these plots is just this transformed patchy saturation line.

When  $A = 0$  in (13) [which seems to happen rarely if ever in the real data examples, but needs to be considered in general], the resulting transformed line will just be one of constant  $\rho/\lambda = B^{-1}$ , which is a vertical line on the  $(\rho/\lambda, \mu/\lambda)$ -plane. The more interesting special case is when  $B = 0$ , in which situation  $\lambda/\mu = A$  or  $\mu/\lambda = A^{-1}$ . But this case includes that of Gassmann-Domenico for homogeneous mixing of the fluids at low to moderate saturation values. For  $B = 0$ , on both planes we have horizontal straight lines, but their lengths can differ significantly on the two displays.

## Interpreting the data point locations

### *Data points inside the triangle*

The triangle described in Section 3.3 provides rigorous bounds on mechanical properties of porous media. For plots in the  $(\rho/\mu, \lambda/\mu)$ -plane such as those included in Figure 1(d) and Figures 3(b), 3(d), and 3(f), some data points lie between the ideal patchy saturation line and the Gassmann ideal lower bound. The relative position of the data points may contain information about the fluid distribution. Consider the case of a core sample that is nearly saturated, above 90% for example. If the weight of the core is used to determine the saturation but the core contains a few gas bubbles, the background saturation will be underestimated and the bubbles themselves represent patches. This is an example of a material having a few isolated patches contained in an otherwise homogeneous partially-saturated background. Such data would plot above but close to the Gassmann curve. In an analogous case for field seismic data, the background saturation may be known from measurements made at lower frequencies or in a nearby region, and it may be possible to use such information to determine the relative volume of patches. For data lying in the middle (*i.e.*, between the bounding curves), some assumptions about fluid distribution could be made and then various estimates about patchy volumes could be applied to different models such as the Hashin-Shtrikman bounds (Hashin and Shtrikman, 1962) or effective medium theories. Exploration of these issues will be the subject of future work.

### *Data points outside the triangle*

The sides of the triangle described above set rigorous boundaries for effects associated with homogeneous saturation and patchy saturation at low frequencies or for situations in which frequency-dependent dispersion can be neglected. However, when the data do not in fact satisfy these assumptions of the theory, plotting the data this way provides an opportunity to observe and interpret deviations from the behavior predicted by the theory. For example, data

which plot above the patchy saturation line represent excessively stiff rock. One possible cause of systematically high stiffness values is frequency-dependent dispersion (Biot, 1956a,b; Biot, 1962; O'Connell and Budiansky, 1977; Mavko and Nur, 1978; Berryman, 1981; McCann and McCann, 1985; Johnson *et al.*, 1987; Norris, 1993; Best and McCann, 1995). Chemical effects, not taken into account in the analysis, might also cause measurements to deviate systematically from predicted behavior. For example, adhesive effects associated with chemical reactions between pore fluid and solid constituents might cause systematically high values. Another consequence of rock-water interactions is softening of intragranular cements. In this case, data for susceptible rocks would systematically plot below the Gassmann line at low saturations. Direct indications from elastic data of rock-water interactions [*e.g.*, see Bonner *et al.* (1997)] may lead to new methods of determining other rock properties controlled by chemical effects, such as the tensile strength.

## CONCLUSIONS

We have shown that seismic/sonic velocity data can be transformed to polar coordinates that have quasi-orthogonal dependence on saturation and porosity. This observation is based on the Gassmann-Domenico relations, which are known to be valid at low frequencies. The transformation loses its effectiveness at high frequencies whenever dispersion becomes significant, because then Biot theory and/or other effects play important roles in determining the velocities. So, the simple relations between  $v_p$ ,  $v_s$ , and  $\lambda$ ,  $\mu$ ,  $\rho$ , and  $S$  break down at high frequencies. Our results are, nevertheless, quite encouraging because the predicted relationships seem to work in many cases up to frequencies of 1 kHz, and in a few special cases to still higher frequencies. These results present a straightforward method for obtaining porosity, saturation, and some information about spatial distribution of fluid (*i.e.*, patchy versus homogeneous) in porous rocks and sediments, from compressional and shear wave velocity data alone. These results have potential applications in various areas of interest, including petroleum exploration and reservoir characterization, geothermal resource evaluation, environmental restoration monitoring, and geotechnical site characterization. The methods may also provide physical insight suggesting new approaches to AVO data analysis.

## ACKNOWLEDGMENTS

We thank Bill Murphy and Rosemarie Knight for providing access to their unpublished data files. We thank Carmen Mora for helpful comments on the text. We thank Norman H. Sleep for his insight clarifying the significance of our sorting method for plotting seismic data.

## REFERENCES

- Aki, K., and Richards, P. G., 1980, *Quantitative Seismology: Theory and Methods*, Vols. I & II, W. H. Freeman and Company, New York.

- Berge, P. A., Bonner, B. P., and Berryman, J. G., 1995, Ultrasonic velocity-porosity relationships for sandstone analogs made from fused glass beads: *Geophysics* **60**, 108–119.
- Berryman, J. G., 1981, Elastic wave propagation in fluid-saturated porous media: *J. Acoust. Soc. Am.* **69**, 416–424.
- Berryman, J. G., 1999, Origin of Gassmann's equations: *Geophysics* **64**, 1627–1629.
- Berryman, J. G., Grechka, V. Y., and Berge, P. A., 1999, Analysis of Thomsen parameters for finely layered VTI media: *Geophys. Prospect.* **47**, 959–978.
- Berryman, J. G., Thigpen, L., and Chin, R. C. Y., 1988, Bulk elastic wave propagation in partially saturated porous solids: *J. Acoust. Soc. Am.* **84**, 360–373.
- Best, A. I., and McCann, C., 1995, Seismic attenuation and pore-fluid viscosity in clay-rich reservoir sandstones: *Geophysics* **60**, 1386–1397.
- Biot, M. A., 1956a, Theory of propagation of elastic waves in a fluid-saturated porous solid. I. Low-frequency range: *J. Acoust. Soc. Am.* **28**, 168–178.
- Biot, M. A., 1956b, Theory of propagation of elastic waves in a fluid-saturated porous solid. II. Higher frequency range: *J. Acoust. Soc. Am.* **28**, 179–1791.
- Biot, M. A., 1962, Mechanics of deformation and acoustic propagation in porous media: *J. Appl. Phys.* **33**, 1482–1498.
- Biot, M. A., and Willis, D. G., 1957, The elastic coefficients of the theory of consolidation: *J. Appl. Mech.* **24**, 594–601.
- Bonner, B. P., Hart, D. J., Berge, P. A., and Aracne, C. M., 1997, Influence of chemistry on physical properties: Ultrasonic velocities in mixtures of sand and swelling clay (abstract): LLNL report UCRL-JC-128306abs, *Eos, Transactions of the American Geophysical Union* **78**, Fall Meeting Supplement, F679.
- Bourbié, T., Coussy, O., and Zinszner, B., 1987, *Acoustics of Porous Media*, Gulf Publishing, Houston, Texas, pp. 56.
- Brown, R. J. S., and Korringa, J., 1975, On the dependence of the elastic properties of a porous rock on the compressibility of the pore fluid: *Geophysics* **40**, 608–616.
- Cadoret, T., 1993, *Effet de la saturation eau/gaz sur les propriétés acoustiques des roches, Étude aux fréquences sonores et ultrasonores*. Ph.D. Dissertation, Université de Paris VII, Paris, France.
- Cadoret, T., Marion, D., and Zinszner, B., 1995, Influence of frequency and fluid distribution on elastic wave velocities in partially saturated limestones: *J. Geophys. Res.* **100**, 9789–9803.
- Cadoret, T., Mavko, G., and Zinszner, B., 1998, Fluid distribution effect on sonic attenuation in partially saturated limestones: *Geophysics* **63**, 154–160.

- Castagna, J. P., and Backus, M. M., 1993, *Offset-Dependent Reflectivity – Theory and Practice of AVO Analysis*, Society of Exploration Geophysicists, Tulsa, OK.
- Castagna, J. P., Batzle, M. L., and Eastwood, R. L., 1985, Relationship between compressional-wave and shear-wave velocities in clastic silicate rocks: *Geophysics* **50**, 571–581.
- Domenico, S. N., 1974, Effect of water saturation on seismic reflectivity of sand reservoirs encased in shale: *Geophysics* **39**, 759–769.
- Dvorkin, J., and Nur, A., 1998, Acoustic signatures of patchy saturation: *Int. J. Solids Struct.* **35**, 4803–4810.
- Endres, A. L., and Knight, R., 1989, The effect of microscopic fluid distribution on elastic wave velocities: *Log Anal.* **30**, 437–444.
- Foster, D. J., Keys, R. G., and Schmitt, D. P., 1997, Detecting subsurface hydrocarbons with elastic wavefields: *Inverse Problems in Wave Propagation*, edited by G. Chavent, G. Papanicolaou, P. Sacks, and W. Symes, Springer, New York, pp. 195–218.
- Gassmann, F., 1951, Über die elastizität poröser medien: *Vierteljahrsschrift der Naturforschenden Gesellschaft in Zürich*, **96**, 1–23.
- Harris, J. M., Nolen-Hoeksema, R. C., Langan, R. T., Van Schaack, M., Lazaratos, S. K., and Rector, J. W., III, 1995, High-resolution crosswell imaging of a west Texas carbonate reservoir: Part 1–Project summary and interpretation: *Geophysics* **60**, 667–681.
- Hashin, Z., and Shtrikman, S., 1962, A variational approach to the theory of elastic behaviour of polycrystals: *J. Mech. Phys. Solids* **10**, 343–352.
- Hill, R., 1952, The elastic behaviour of crystalline aggregate: *Proc. Phys. Soc. London A* **65**, 349–354.
- Johnson, D. L., J. Koplik, and R. Dashen, Theory of dynamic permeability and tortuosity in fluid-saturated porous-media: *J. Fluid Mech.* **176**, 379–402 (1987).
- Knight, R., and Nolen-Hoeksema, R., 1990, A laboratory study of the dependence of elastic wave velocities on pore scale fluid distribution: *Geophys. Res. Lett.* **17**, 1529–1532.
- Mavko, G., and Nolen-Hoeksema, R., 1994, Estimating seismic velocities at ultrasonic frequencies in partially saturated rocks: *Geophysics* **59**, 252–258.
- Mavko, G. M., and Nur, A., 1978, The effect of nonelliptical cracks on the compressibility of rocks: *Geophysics* **83**, 4459–4468.
- McCann, C., and McCann, D. M., 1985, A theory of compressional wave attenuation in non-cohesive sediments: *Geophysics* **50**, 1311–1317.
- Murphy, William F., III, 1984, Acoustic measures of partial gas saturation in tight sandstones: *J. Geophys. Res.* **89**, 11549–11559.

- Norris, A. N., 1993, Low-frequency dispersion and attenuation in partially saturated rocks: *J. Acoust. Soc. Am.* **94**, 359–370.
- Nur, A., and Simmons, G., 1969, The effect of saturation on velocity in low porosity rocks: *Earth and Planet. Sci. Lett.* **7**, 183–193.
- O’Connell, R. J., and Budiansky, B., 1977, Viscoelastic properties of fluid-saturated cracked solids: *J. Geophys. Res.* **82**, 5719–5736.
- Ostrander, W. J., 1984, Plane-wave reflection coefficients for gas sands at non-normal angles of incidence: *Geophysics* **49**, 1637–1648.



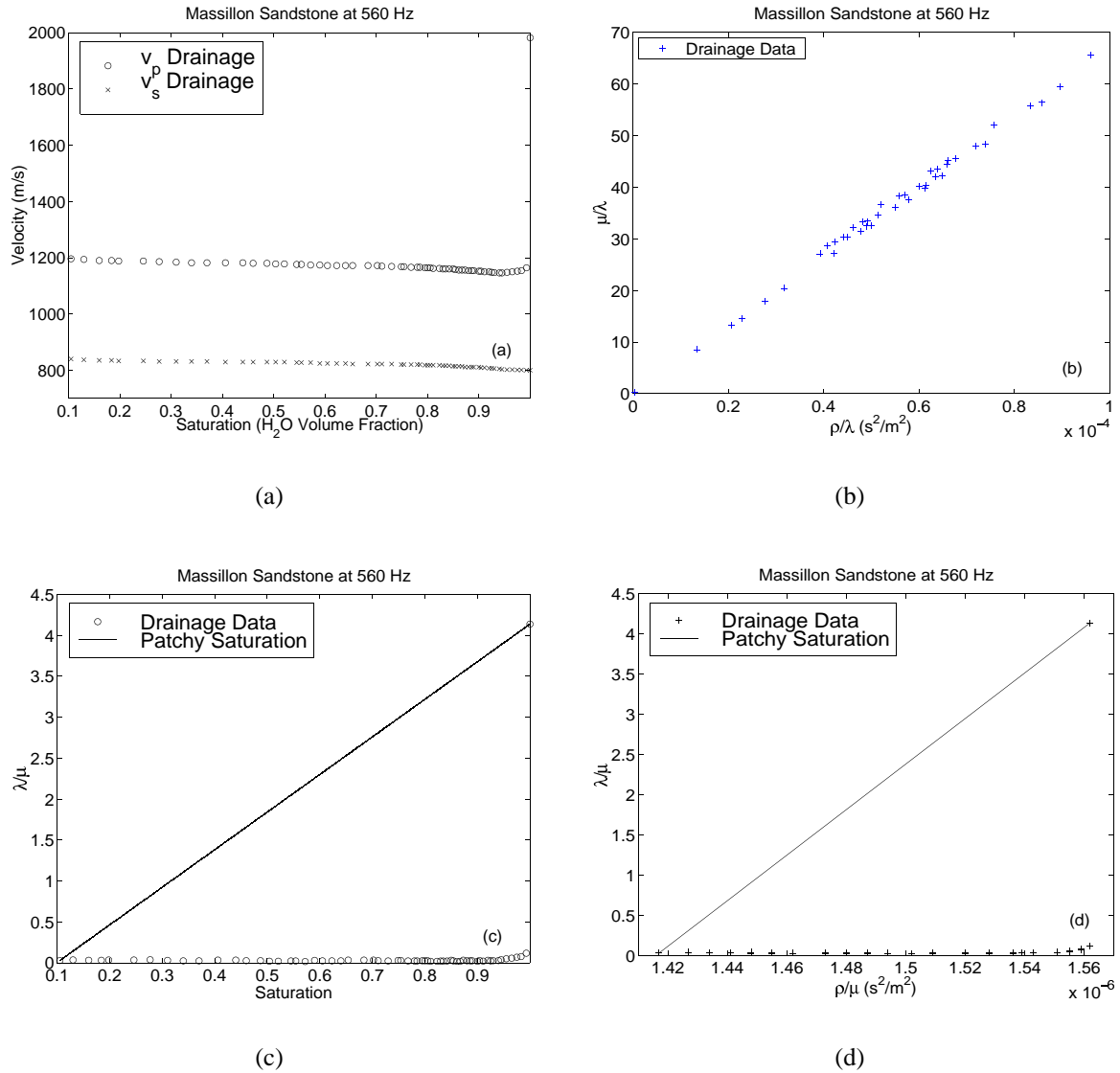


Figure 1: Various methods of plotting 560 Hz Massillon sandstone data of Murphy (1984): (a) Compressional and shear wave velocities as a function of saturation, (b) transform to  $(\rho/\lambda, \mu/\lambda)$ -plane, (c)  $\lambda/\mu$  versus saturation, (d) transform to  $(\lambda/\mu, \rho/\mu)$ -plane. All of these behaviors are anticipated by the Gassmann-Domenico relations for homogeneously mixed fluid in the pores.

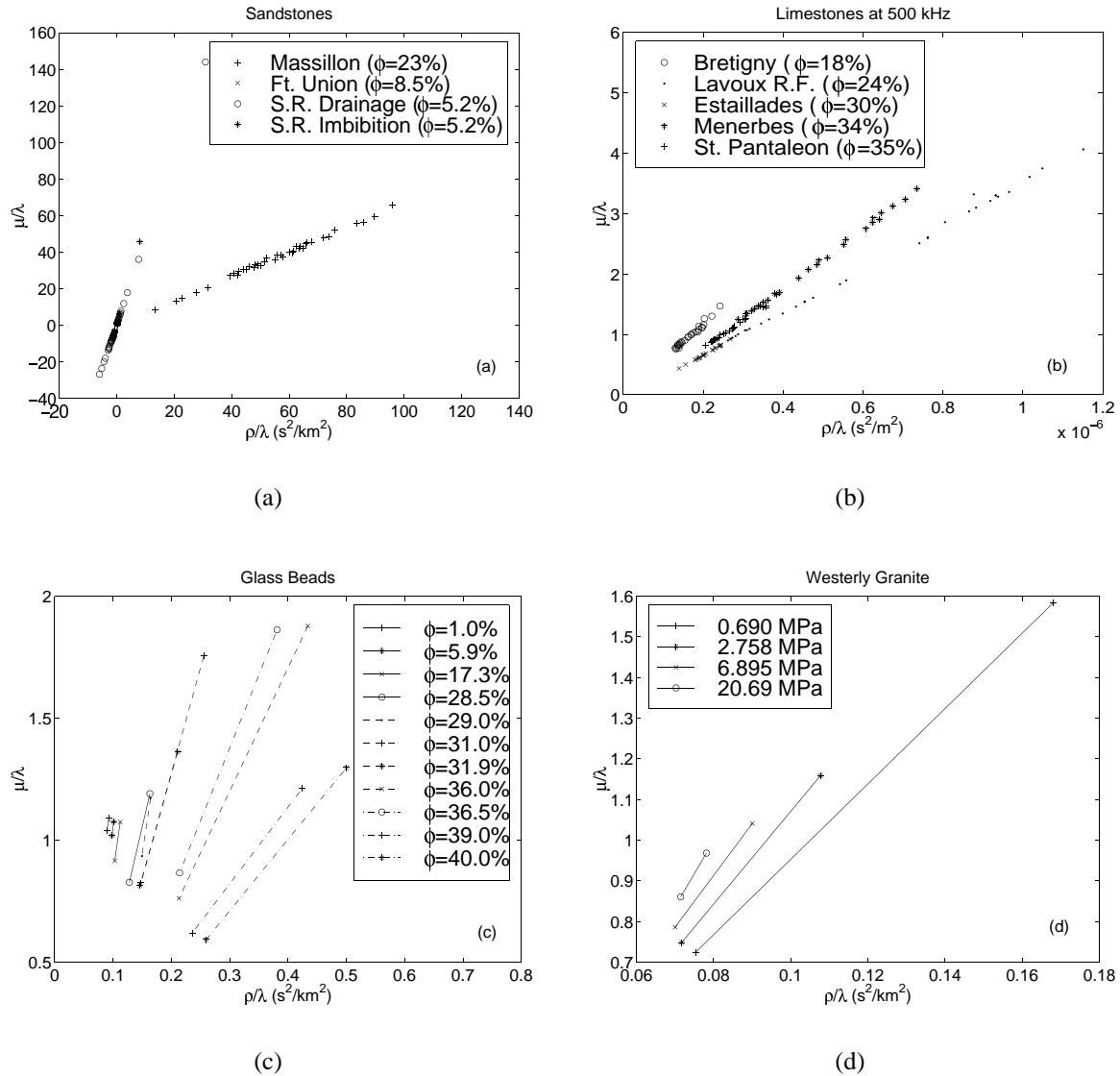


Figure 2: Examples of the correlation of slopes with porosity in the data-sorting plots: (a) three Spirit River (S.R.) sandstone (Knight and Nolen-Hoeksema, 1990) and Massillon and Ft. Union sandstones (Murphy, 1984), (b) five limestones (Cadoret *et al.*, 1998), (c) 11 fused glass-bead samples (Berge *et al.*, 1995), (d) Westerly granite (Nur and Simmons, 1969) at four pressures. The observed trend is that high porosity samples generally have lower slopes than lower porosities on these plots, although there are a few exceptions as discussed in the text. These trends are easily understood since the slopes are determined approximately by the average value of  $v_s^2$  for each material, which is a decreasing function of porosity  $\phi$ .

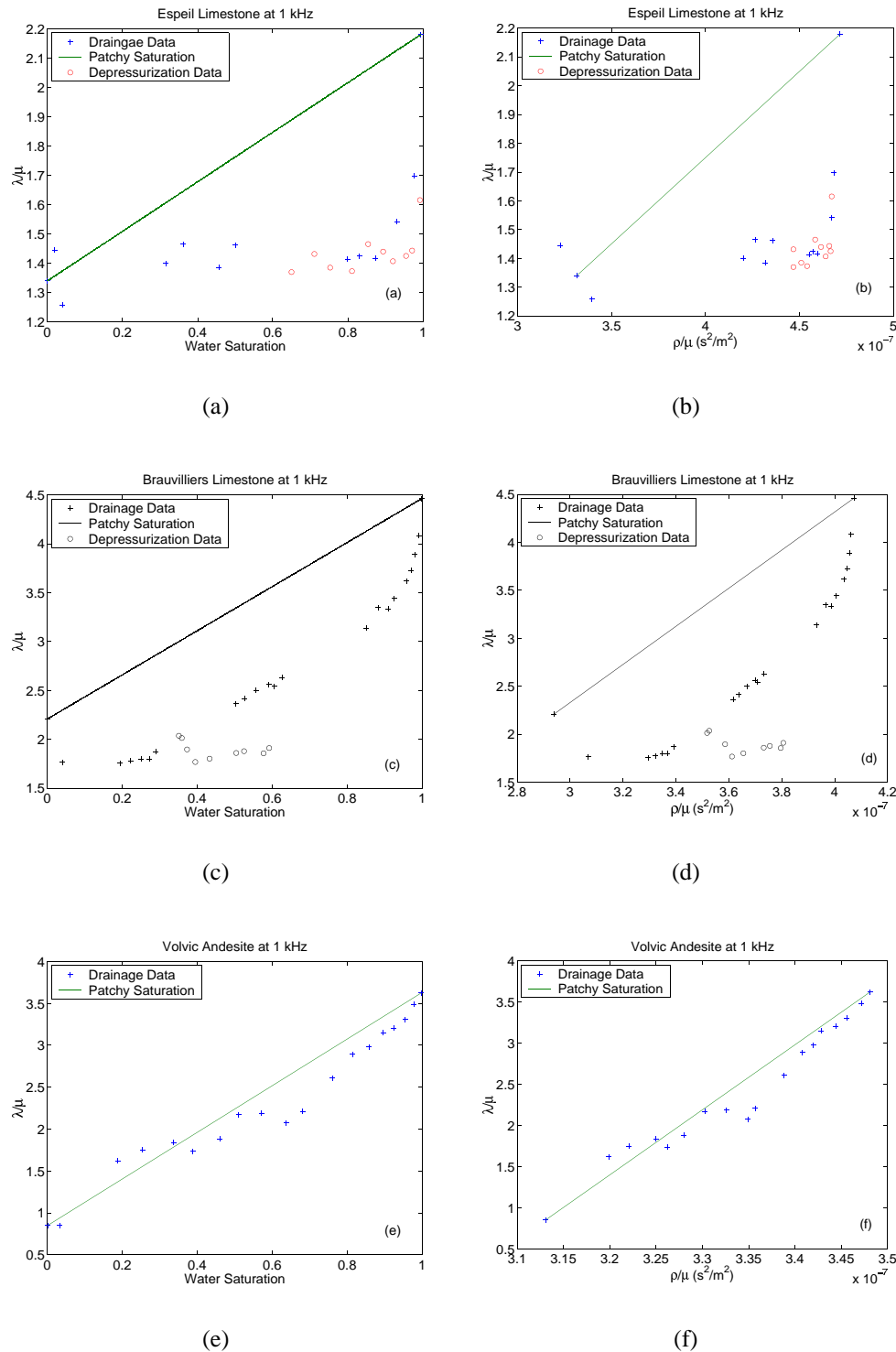


Figure 3: Lamé parameter ratio  $\lambda/\mu$  plotted versus (a) saturation and (b)  $\rho/\mu$  for Espelil limestone, (c) saturation and (d)  $\rho/\mu$  for Brauvilliers limestone, and (e) saturation and (f)  $\rho/\mu$  for Volvic andesite. All extensional and shear wave measurements (Cadoret, 1993; Cadoret *et al.*, 1995; 1998) were made at 1 kHz. Note that (a) and (b) indicate homogeneous mixing of liquid and gas, (e) and (f) indicate extremely patchy mixing, while (c) and (d) show an intermediate state of mixing for the drainage data, but more homogeneous mixing for the depressurization data. The plots on the right are saturation-proxy plots, having essentially the same behavior as the plots on the left but requiring only velocity data.

